Dalton Transactions

ROYAL SOCIETY OF CHEMISTRY

PAPER

View Article Online
View Journal | View Issue



Cite this: *Dalton Trans.*, 2025, **54**, 6674

# Synthesis and X-ray structure analysis of cytotoxic 2-picolylamino-type $Hf^{IV}$-bis-chelated complexes†

Tiankun Zhao, *‡[a,b] Qi Zhang,‡[a] Jialiu Zhao,‡[a] Dongyu Mei,[a] Jing Ma,[a] Isabel Correia, [b] Zhongduo Yang,[a] Sa-Hyun Kim[c] and Thomas Huhn *[d]

Received 12th October 2024,
Accepted 18th March 2025

DOI: 10.1039/d4dt02859g

rsc.li/dalton

Eight novel heteroleptic $Hf^{IV}$ complexes containing differently substituted 2-picolylamino-bis-phenolate and 2,6-dipicolinic acid (Dipic) groups as chelating ligands were synthesized and characterized with yields higher than 80%. These [ONON] type $Hf^{IV}$ complexes have good aqueous stability and potent anti-tumor activity against HeLa S3 (human cervical adenocarcinoma) and Hep G2 (human derived hepatoma) cells. In particular, the complexes demonstrated selective inhibitory activity against Hep G2 cells. The $IC_{50}$ value of the most cytotoxic complex **[$L_1Hf^{IV}Dipic^{4\text{-}Cl}$]** (0.9 ± 0.4 μM) was ten-fold higher than that of cisplatin (11.2 ± 2.1 μM) on Hep G2 cells, being the most cytotoxic anti-tumor $Hf^{IV}$ complex to date. Furthermore, **[$L_1Hf^{IV}Dipic^{4\text{-}Cl}$]** could inhibit tumor cell migration, induce reactive oxygen species generation (particularly $HO^{\bullet}$), loss of mitochondrial membrane potential and almost exclusive early apoptosis in HeLa S3 cells. **[$L_1Hf^{IV}Dipic^{4\text{-}Cl}$]** exhibited rapid cellular uptake by HeLa S3 cells, and when in aqueous media, these $Hf^{IV}$ complexes slowly hydrolyzed, releasing non-toxic phenolato ligands as the product of hydrolysis. Overall, these rare earth complexes, particularly **[$L_1Hf^{IV}Dipic^{4\text{-}Cl}$]**, show promising potential as novel anti-cancer agents with significant efficacy against human liver cancer cells and favorable selectivity profiles for further therapeutic development.



## Introduction

Titanocene dichloride (**[$Cp_2Ti^{IV}Cl_2$]**, TDC) and budotitane (bis-(1-phenyl-1,3-butanedione)$Ti^{IV}$) were the first group 4 metal complexes with anti-tumor activity reported in the 1980s.[1,2] Both entered clinical trials but failed due to limited aqueous stability and undefined mechanisms of action. Still, they opened a new chapter in medicinal chemistry as a large number of their derivatives have been synthesized and evaluated for anti-tumor efficacy over the last decades.[3] In 2007, Tshuva *et al.* reported a di-amino-phenolato $Ti^{IV}$ bis-alkoxyl complex that exhibited significantly improved aqueous stability and stronger anti-tumor activity than TDC,[4] thus laying the foundation for a new generation of anti-tumor $Ti^{IV}$ complexes.[5,6] Following studies, by us[7,8] and others,[9,10] it was shown that the aqueous stability can be further improved by replacing the labile alkoxy groups on $Ti^{IV}$ with additional chelators. These can either be part of the phenolato backbone (*N*-hydroxyethyl), resulting in homoleptic complexes, or achieved by introducing an additional chelator (2,6-dipicolinic acid, Dipic), resulting in heteroleptic $Ti^{IV}$ complexes. These heteroleptic $Ti^{IV}$ complexes have significantly enhanced kinetic stability and anti-tumor activity. The anti-tumor active species formed by hydrolysis,[11] the *in vivo* anti-tumor efficacy[12] and the mechanism of action were subsequently investigated.[13,14]

In addition to their role as potential anti-tumor candidates, the above heteroleptic Ti-complexes have recently found application in tumor sensing and as tumor targeting drugs.[15] A $^{45}Ti$ complex stabilized by the above heteroleptic ligand system has recently been used as a PET (positron emission tomography) tracer to visualize tumor tissue. Conjugation of a Dipic-based heteroleptic $^{45}Ti$ complex with tumor targeting PSMA (prostate specific membrane antigen) has combined chemotherapeutic effects with diagnostic features.[16]

Recently, we reported a post-functionalization protocol for **[(Salan)$Ti^{IV}$(Dipic)]** *via* a pallidum-catalyzed Sonogashira reaction,[17] and an environmentally benign synthesis of heteroleptic bis-chelated $Ti^{IV}$ complexes in green solvents within minutes.[18] Since SAR (structure–activity relationship) data

[a]*School of Life Science and Engineering, Lanzhou University of Technology, Lanzhou, 730050, China. E-mail: tiankun.zhao@tecnico.ulisboa.pt, zhaotiankun2006@163.com*
[b]*Centro de Química Estrutural and Departamento de Engenharia Química, Institute of Molecular Sciences, Instituto Superior Técnico, Avenida Rovisco Pais 1, 1049-001 Lisboa, Portugal*
[c]*Department of Clinical Laboratory Science, Kyungpook National University, Daegu, 27136, South Korea*
[d]*Fachbereich Chemie, Universität Konstanz, Universitätsstr. 10, D-78457 Konstanz, Germany*

†Electronic supplementary information (ESI) available. CCDC 2390816 and 2390817. For ESI and crystallographic data in CIF or other electronic format see DOI: https://doi.org/10.1039/d4dt02859g

‡These authors have contributed equally to this work.

revealed that the phenolato "part" is crucial for the anti-tumor activity of Salan-type $Ti^{IV}$ complexes,[19] we further expanded the complex library to three types of phenolato ligands: [ONNO] (Salan) type, [ONON] type with a 2-picolylamino "side bridge" and [ONOO] type with an *N*-(2-hydroxyethyl) "side arm". Among them, the [ONON] type $Ti^{IV}$ complexes showed the strongest anti-tumor activity and low toxicity on primary cells.[13] Despite the above achievements for anti-tumor $Ti^{IV}$ complexes, the field for the other two group 4 metals, Zr (Zirconium) and Hf (Hafnium), is surprisingly underdeveloped. In particular, to the best of our knowledge, for anti-tumor $Hf^{IV}$ complexes, only 10 related reports have been found.

Coordination complexes of rare earth metals, especially those of hafnium, have been mainly used in luminescent materials[20,21] and as catalysts for polymerization reactions.[22–25] Regarding bioactive $Hf^{IV}$ complexes, early reports showed that hafnocene dichloride did not exhibit anti-tumor activity.[26] A folate–$Hf^{IV}$ conjugate showed anti-bacterial and anti-fungal activity.[27] In contrast, McGowan *et al.* reported that the $IC_{50}$ of a tris-diphenyl β-diketonato $Hf^{IV}$ complex was in the same range as that of cisplatin against HT-29 (human colorectal adenocarcinoma) and MCF-7 (Michigan Cancer Foundation-7, human breast adenocarcinoma). However, its aqueous stability was not investigated,[28] probably for the same reasons that budotitane failed earlier. Recently, Choi *et al.* reported that a Hf-MOF (metal organic framework) containing a folate moiety could generate ROS (reactive oxygen species), deregulate tumor-cell proliferation, as well as increase apoptosis.[29] We recently reported four Salan-type $Hf^{IV}$ complexes containing Dipic derivatives as the second chelator.[30] The complex with Dipic substituted with Cl at position 4 showed rapid cellular uptake and induced almost exclusively apoptosis in HeLa S3 cells (human cervical adenocarcinoma). Furthermore, an oxo-bridged dimeric $Hf^{IV}$–$Hf^{IV}$ complex was identified as a novel anti-tumor compound.[31] In contrast to Hf-based nanomaterials, which have been intensively studied,[32,33] molecular $Hf^{IV}$ complexes are rather scarce, with only four representatives of $Hf^{IV}$ bis-chelates known to date. We report herein the synthesis and characterization of eight new $Hf^{IV}$ bis-chelates with tripodal tetradentate [ONON]-type ligands, $H_2L_{1-4}$ bearing a 2-picolylamino side bridge (Scheme 1). Their *in vitro* anti-tumor activity and mechanism of cellular uptake, ROS production and apoptosis are also investigated and presented.

# Results and discussion

## Synthesis and molecular structure

The SAR (structure–activity relationship) from our previous report on phenolato $Ti^{IV}$ bis-chelates indicated that the aqueous stability and anti-tumor activity of the complexes were dominated by the substitution pattern on the phenolato moiety.[13] When the 2 position of the phenyl (phenolato) was occupied by sterically demanding groups, such as *t*-butyl, the stability was significantly enhanced. While cytotoxicity was maintained for 2-picolylamino and 2-hydroxyethylamino $Ti^{IV}$ complexes, it disappeared for Salan $Ti^{IV}$ complexes bearing the ethylenediamino linker. Less bulky substitutions such as those with methyl were important for both cytotoxicity and stability. Lighter halogen atoms, such as Cl and F, increased the cytotoxicity, whereas Br decreased it. Additionally, our previous work with $Hf^{IV}$ complexes showed that the Cl atom on the Dipic co-ligand was also important, since it enhanced the compound's polarity and provided the necessary solubility in polar solvents.[30]

Based on the above observations, ligands $H_2L_{1-4}$ containing *t*-butyl and methyl at the 2, 3 and 4 positions (phenyl) were synthesized, and $Dipic^{4\text{-Cl}}$ was also employed as a second chelator. It is worth mentioning that 2-picolylamino ligands bearing halogens could not be converted into the corresponding $Hf^{IV}$ complexes and were therefore excluded from this study. **[$L_{1-4}Hf^{IV}Dipic^{4\text{-H,Cl}}$]** complexes were easily synthesized from $Hf(O^nBu)_4$ in toluene, following our previous report,[30] and in good yields (>80%). The $Hf^{IV}$ complexes of $H_2L_2$ and $H_2L_3$ containing *t*-butyl in the *ortho* position to the OH group could be purified directly by flash chromatography on silica gel, whereas the $Hf^{IV}$ complexes of $H_2L_1$ and $H_2L_4$ are kinetically less stable and decompose on silica gel. For these, purification relied on filtration of insoluble matter and washing with toluene to remove unreacted ligands. The enhanced stability with increasing bulkiness at the *ortho* position is a direct consequence of steric shielding of the O–Ti bond.[19] All ligands and $Hf^{IV}$ complexes were characterized by the usual analytical techniques of $^1H$ and $^{13}C$ NMR, FTIR, HRMS (ESI-TOF), elemental analysis and UV-vis absorption spectroscopy and details are given in the ESI.† These confirm the molecular structure of the compounds and their purity. The HPLC analyses (see the ESI†) show, for all complexes, the

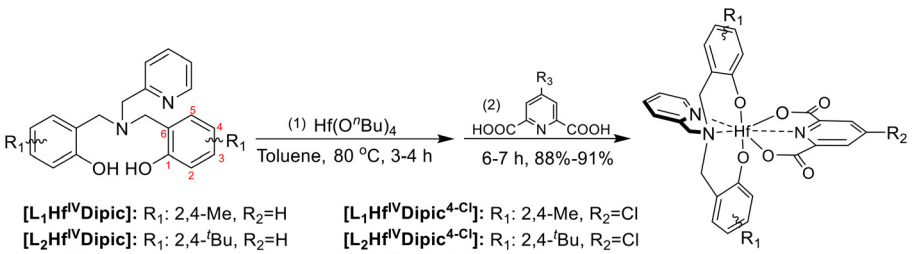


**[$L_1Hf^{IV}Dipic$]:** $R_1$: 2,4-Me, $R_2$=H
**[$L_2Hf^{IV}Dipic$]:** $R_1$: 2,4-$^t$Bu, $R_2$=H
**[$L_3Hf^{IV}Dipic$]:** $R_1$: 2-$^t$Bu, 4-Me, $R_2$=H
**[$L_4Hf^{IV}Dipic$]:** $R_1$: 3,4-Me, $R_2$=H

**[$L_1Hf^{IV}Dipic^{4\text{-Cl}}$]:** $R_1$: 2,4-Me, $R_2$=Cl
**[$L_2Hf^{IV}Dipic^{4\text{-Cl}}$]:** $R_1$: 2,4-$^t$Bu, $R_2$=Cl
**[$L_3Hf^{IV}Dipic^{4\text{-Cl}}$]:** $R_1$: 2-$^t$Bu, 4-Me, $R_2$=Cl
**[$L_4Hf^{IV}Dipic^{4\text{-Cl}}$]:** $R_1$: 3,4-Me, $R_2$=Cl

**Scheme 1** Synthesis of 2-picolylamino [ONON]-type $Hf^{IV}$ bis-chelates **[$L_{1-4}Hf^{IV}Dipic$]** and **[$L_{1-4}Hf^{IV}Dipic^{4\text{-Cl}}$]**.

presence of one peak, corresponding to >99%, corroborating their high purity.

Single crystals suitable for X-ray diffraction analysis of **[$L_2Hf^{IV}$Dipic]** and **[$L_2Hf^{IV}Dipic^{4\text{-}Cl}$]** were obtained by slow crystallization in a mixed solvent consisting of dichloromethane and hexane (1 : 1) at −20 °C. The solid state ORTEP diagrams of the molecular structures are depicted in Fig. 1. The main crystallographic data and selected bond distances and angles are given in the ESI.† **[$L_2Hf^{IV}$Dipic]** is triclinic and **[$L_2Hf^{IV}Dipic^{4\text{-}Cl}$]** is monoclinic and they crystallized in $P\bar{1}$ and $P2_{1/n}$ space groups, respectively. The **[$L_2Hf^{IV}$Dipic]** unit cell also contains one molecule of hexane and one molecule of $H_2O$. Similar to the reported [ONNO]-type (Salan) **[$L_5Hf^{IV}$Dipic]** ($L_5$ = 6,6′-((ethane-1,2-diylbis(methylazanediyl))bis(methylene))bis(2,4-dimethylphenol)),[30] the tripodal [ONON]-type ligand occupies one face of a pseudo-octahedron with Dipic occupying the remaining *cis*-positions, forming a hepta-coordination sphere around the $Hf^{IV}$ centre. The bond angles of O(1)–Hf–O(2) (161.31° and 162.93°) and O(3)–Hf–O(4) (137.06° and 137.91°) of **[$L_2Hf^{IV}$Dipic]** and **[$L_2Hf^{IV}Dipic^{4\text{-}Cl}$]** are all smaller than those of **[$L_5Hf^{IV}$Dipic]** (168.33° and 138.52°), due to the tripodal arrangement of $L_2$. However, the 2-picolylamino side bridge does not significantly affect the N(1)–Hf–N(2) angle (Table 1). Finally, the dihedral angle of the phenyl moieties in **[$L_5Hf^{IV}$Dipic]** (78.44°) is much larger than in **[$L_2Hf^{IV}$Dipic]** and **[$L_2Hf^{IV}Dipic^{4\text{-}Cl}$]** (49.3° and 48.7°) (Fig. S3†). This rather "flat" arrangement of the phenyl rings reflects to some extent the spatial flexibility of the 2-picolylamino $Hf^{IV}$ complexes.

Additionally, PXRD (powder X-ray diffraction) was performed on **[$L_2Hf^{IV}$Dipic]** and **[$L_2Hf^{IV}Dipic^{4\text{-}Cl}$]**, and the obtained spectra are consistent with the simulated ones (Fig. S4†), suggesting a pure phase for the two Hf-based crystals.

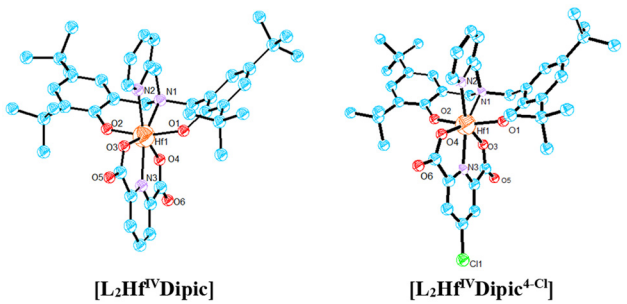


**[$L_2Hf^{IV}$Dipic]** **[$L_2Hf^{IV}Dipic^{4\text{-}Cl}$]**

**Fig. 1** Solid state molecular structures of approximate $C_2$ symmetric hepta-coordinated [ONON]-type $Hf^{IV}$ bis-chelates. Thermal ellipsoids are drawn at the 50% probability level. Hydrogen atoms are omitted for clarity.

**Table 1** Selected bond lengths (Å) and angles (°) of **[$L_2Hf^{IV}$Dipic]** and **[$L_2Hf^{IV}Dipic^{4\text{-}Cl}$]** and a previously reported **[$L_5Hf^{IV}$Dipic]** [30]

| | [$L_2Hf^{IV}$Dipic] | [$L_2Hf^{IV}Dipic^{4\text{-}Cl}$] | [$L_5Hf^{IV}$Dipic] |
|---|---|---|---|
| O(1)–Hf | 1.980(19) | 1.998(3) | 1.985(2) |
| O(2)–Hf | 1.983(19) | 1.969(3) | 1.988(2) |
| O(3)–Hf | 2.133(19) | 2.156(3) | 2.121(2) |
| O(4)–Hf | 2.149(19) | 2.116(3) | 2.135(2) |
| N(1)–Hf | 2.398(2) | 2.402(4) | 2.432(3) |
| N(2)–Hf | 2.394(2) | 2.427(4) | 2.420(3) |
| N(3)–Hf | 2.292(2) | 2.282(4) | 2.283(3) |
| O(1)–Hf–O(2) | 161.31(8) | 162.93(14) | 168.33(9) |
| O(3)–Hf–O(4) | 137.06(7) | 137.91(12) | 138.52(9) |
| N(1)–Hf–N(2) | 71.11(8) | 70.51(13) | 72.67(9) |

## Stability and hydrolysis

The aqueous stability of the synthesized $Hf^{IV}$ complexes was investigated in a mixed solvent of 1/10 (v/v) of $H_2O$/THF ($H_2O$ calculated to be $1 \times 10^5$ equiv.) by time-resolved UV-vis spectroscopy at 37 °C. As shown in Table 2, **[$L_1Hf^{IV}$Dipic]**, **[$L_1Hf^{IV}Dipic^{4\text{-}Cl}$]**, **[$L_4Hf^{IV}$Dipic]** and **[$L_4Hf^{IV}Dipic^{4\text{-}Cl}$]** decomposed rather slowly with $t_{1/2}$ (half-hydrolyzation time) calculated to be 20 h, 10 h, 20 h and 15 h, respectively. The stability characteristics of these [ONON]-type $Hf^{IV}$ complexes are similar to those of the Salan $Hf^{IV}$ bis-chelates, as evidenced by the complexes of $L_2$ and $L_3$ with at least one *t*-butyl *ortho* to the phenolato oxygen, which remained stable (see the ESI, Fig. S9–S16†) in the time frame studied. Moreover, the products of hydrolysis of **[$L_1Hf^{IV}Dipic^{4\text{-}H,Cl}$]** and **[$L_4Hf^{IV}Dipic^{4\text{-}H,Cl}$]** complexes were isolated from scaled-up reactions at 50 °C and characterized by HRMS (high resolution mass spectrometry) to be $H_2L_1$ and $H_2L_4$, respectively (Fig. S17 and S18 in the ESI†).

## Cytotoxicity assay

The anti-tumor activity of the **[$L_{1\text{–}4}Hf^{IV}Dipic^{4\text{-}H,Cl}$]** complexes and respective ligands was examined by the MTT (methylthiazolyldiphenyl-*tetra*-zolium bromide) assay on HeLa S3 (human cervical carcinoma) and Hep G2 (human derived hepatoma) cells with cisplatin as the reference. The $IC_{50}$ value for each sample was calculated as the average of the data obtained from three experiments on different days. In each replicate, all concentrations were repeated five times.

As shown in Table 3, **[$L_1Hf^{IV}$Dipic]** (entry 1) showed reduced inhibitory activity against the two tumor cell lines compared to cisplatin (entry 15). However, the anti-tumor

**Table 2** Values of $t_{1/2}$ (half-hydrolyzation time) of $Hf^{IV}$ complexes in a 1/10 mixture (v/v) of $H_2O$/THF

| Entry[a] | Complex | $t_{1/2}$ (h) | $\lambda_{max}$[c] (nm) |
|---|---|---|---|
| 1 | **[$L_1Hf^{IV}$Dipic]** | 20 | 343 |
| 2 | **[$L_2Hf^{IV}$Dipic]** | Stable[b] | 288 |
| 3 | **[$L_3Hf^{IV}$Dipic]** | Stable[b] | 343 |
| 4 | **[$L_4Hf^{IV}$Dipic]** | 20 | 343 |
| 5 | **[$L_1Hf^{IV}Dipic^{4\text{-}Cl}$]** | 10 | 343 |
| 6 | **[$L_2Hf^{IV}Dipic^{4\text{-}Cl}$]** | Stable[b] | 295 |
| 7 | **[$L_3Hf^{IV}Dipic^{4\text{-}Cl}$]** | Stable[b] | 343 |
| 8 | **[$L_4Hf^{IV}Dipic^{4\text{-}Cl}$]** | 15 | 343 |

[a] Hydrolysis was followed by time-resolved UV-vis spectroscopy after mixing 3 mL of THF solution of $Hf^{IV}$ complex (13.9 mmol) with 0.3 mL of $H_2O$ (0.3 mL, $1 \times 10^5$ equiv.) at 37 °C. [b] No decomposition after 2 weeks. [c] $\lambda_{max}$ of each $Hf^{IV}$ complex was determined by UV-vis spectroscopy.

**Table 3** $IC_{50}$ values (μM) obtained by the MTT assay in HeLa S3 and Hep G2 cells, after 48 h of incubation

| Entry | Complex | HeLa S3 | Hep G2 |
|---|---|---|---|
| 1 | **[$L_1Hf^{IV}Dipic$]** | 15.1 ± 2.7 | 31.8 ± 9.8 |
| 2 | **[$L_2Hf^{IV}Dipic$]** | Non-toxic | Non-toxic |
| 3 | **[$L_3Hf^{IV}Dipic$]** | Non-toxic | 44.3 ± 0.1 |
| 4 | **[$L_4Hf^{IV}Dipic$]** | Non-toxic | 38.4 ± 18.6 |
| 5 | **[$L_1Hf^{IV}Dipic^{4\text{-Cl}}$]** | 2.2 ± 0.1 | 0.9 ± 0.4 |
| 6 | **[$L_2Hf^{IV}Dipic^{4\text{-Cl}}$]** | 14.4 ± 2.2 | 4.3 ± 1.5 |
| 7 | **[$L_3Hf^{IV}Dipic^{4\text{-Cl}}$]** | 17.3 ± 5.1 | 3.9 ± 1.4 |
| 8 | **[$L_4Hf^{IV}Dipic^{4\text{-Cl}}$]** | 7.3 ± 4.5 | 2.1 ± 0.6 |
| 9 | **[$L_5Hf^{IV}Dipic^{4\text{-Cl}}$]** | 1.5 ± 0.3 | 6.7 ± 1.4 |
| 10 | $H_2L_1$ | Non-toxic[a] | Non-toxic |
| 11 | $H_2L_2$ | Non-toxic | Non-toxic |
| 12 | $H_2L_3$ | Non-toxic | Non-toxic |
| 13 | $H_2L_4$ | Non-toxic[a] | Non-toxic |
| 14 | Dipic and $Dipic^{4\text{-Cl}}$ | Non-toxic | Non-toxic |
| 15 | Cisplatin | 3.5 ± 0.4 | 11.2 ± 2.1 |

[a] Partially active on HeLa S3 cells, see ESI.†

activity of **[$L_2Hf^{IV}Dipic$]** (entry 2) disappeared completely. Interestingly, **[$L_3Hf^{IV}Dipic$]** and **[$L_4Hf^{IV}Dipic$]** demonstrated high selectivity against Hep G2 cells (entries 3 and 4). The introduction of Cl into the Dipic co-ligand significantly increased the anti-tumor activity, and **[$L_{1-4}Hf^{IV}Dipic^{4\text{-Cl}}$]** all showed anti-tumor activity in the low micromolar range against the two tumor cell lines, in some cases higher than cisplatin (entries 5–8). Furthermore, all $Dipic^{4\text{-Cl}}$ complexes are more cytotoxic to Hep G2 than to HeLa S3 cancer cells, and among them **[$L_1Hf^{IV}Dipic^{4\text{-Cl}}$]** is the most cytotoxic complex ($IC_{50}$: 2.2 ± 0.1 μM on HeLa S3; 0.9 ± 0.4 μM on Hep G2). Its $IC_{50}$ value is comparable to the cytotoxic Salan type, **[$L_5Hf^{IV}Dipic^{4\text{-Cl}}$]**[30] (entry 9), and to the structurally related $Ti^{IV}$ complex, **[$L_2Ti^{IV}Dipic$]**.[13] The ligands $H_2L_{1-4}$, Dipic and $Dipic^{4\text{-Cl}}$ were tested separately for cytotoxicity, and except for $H_2L_1$ and $H_2L_4$, which have partial activity on HeLa S3 cells in the concentration range of $1 \times 10^{-7}$ μM to $1 \times 10^{-5}$ μM, the others were all non-toxic (entries 10–14).

From the above results, we can conclude that the 2-picolylamino $Hf^{IV}$ complexes containing $Dipic^{4\text{-Cl}}$ generally have higher anti-tumor activity than the reported Salan-type $Hf^{IV}$ bis-chelates and cisplatin against Hep G2 cells, and that **[$L_1Hf^{IV}Dipic^{4\text{-Cl}}$]** performs better than cisplatin in HeLa S3 cells.

### Structure–activity relationship

The structure–activity (stability) relationship of the phenolato ([ONON] and [ONNO]-type) $Hf^{IV}$ bis-chelates is summarized in Fig. 2. The $Hf^{IV}$ bis-chelates containing Dipic as co-ligand generally exhibit low molecular polarity, resulting in poor solubility in DMSO. The use of $Dipic^{4\text{-Cl}}$ significantly enhances the molecular polarity leading to better solubility and good cytotoxicity. The $Hf^{IV}$ complexes bearing phenolato(*t*-butyl) moieties demonstrated good aqueous stability but insufficient anti-tumor activity. The [ONNO] and [ONON]-type $Hf^{IV}$ complexes containing non-bulky substituents, such as methyl at either the 2 or 3 positions of phenolato, generally showed

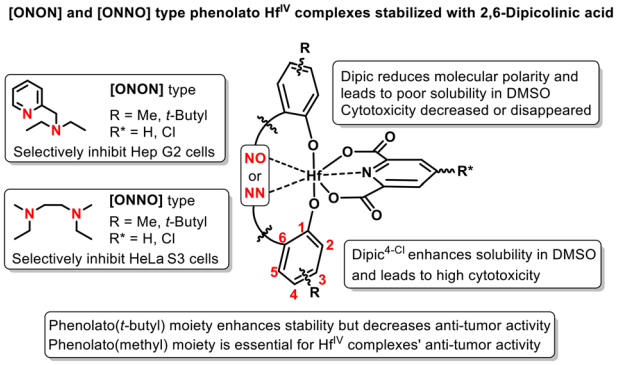


**Fig. 2** Structure–activity relationship of [ONON]-type and [ONNO]-type $Hf^{IV}$ bis-chelates.

good cytotoxicity. In comparison to the [ONNO]-type $Hf^{IV}$ complexes, which selectively inhibit the growth of HeLa S3 cells, the [ONON]-type $Hf^{IV}$ complexes are more prone to inhibit Hep G2 cells. Furthermore, neither methyl nor H at the phenolato-2 position has a significant effect on the aqueous stability.

### Apoptosis assay

Since **[$L_1Hf^{IV}Dipic^{4\text{-Cl}}$]** was the complex with the lowest $IC_{50}$ values, it was selected for studies on the mechanism of action. First, **[$L_1Hf^{IV}Dipic^{4\text{-Cl}}$]** was subjected to apoptotic analysis using the Annexin V-FITC/PI apoptosis assay kit. HeLa S3 cells were used for direct comparison with the [ONNO]-type $Hf^{IV}$ complex, **[$L_5Hf^{IV}Dipic^{4\text{-Cl}}$]**.[30] Cells were treated with $1 \times 10^{-2}$ μM, 1 μM and $1 \times 10^{2}$ μM of **[$L_1Hf^{IV}Dipic^{4\text{-Cl}}$]** for 24 h and were analyzed by flow cytometry. As depicted in Fig. S8,† **[$L_1Hf^{IV}Dipic^{4\text{-Cl}}$]** could induce 17.0%, 19.6% and 23.4% apoptosis in total at the three concentrations in HeLa S3 cells. In comparison to necrosis, apoptosis leads to significantly reduced side effects and is therefore preferred for anti-tumor drugs. In our study, **[$L_1Hf^{IV}Dipic^{4\text{-Cl}}$]** induced only 1.3%, 1.6% and 1.3% necrosis of HeLa S3 cells at the tested concentrations (1.4% necrotic cells observed in the control group) (Fig. 3). Next, the apoptosis levels in Hep G2 cells were investigated using **[$L_1Hf^{IV}Dipic^{4\text{-Cl}}$]**, **[$L_5Hf^{IV}Dipic^{4\text{-Cl}}$]** and **[$L_2Ti^{IV}Dipic$]** aiming to gain more insights into their cytotoxicity behavior (Fig. 3 and Fig. S7†). The results indicate that the three metal complexes could almost exclusively induce apoptosis in Hep G2 cells, with a percentage of apoptotic cells in dead cells of 26.9%, 17.1% and 32.3% at $1 \times 10^{2}$ μM, respectively (Fig. S8†). A closer look at all data also shows that **[$L_1Hf^{IV}Dipic^{4\text{-Cl}}$]** and **[$L_5Hf^{IV}Dipic^{4\text{-Cl}}$]** induce more early apoptosis than late apoptosis on both HeLa S3 and Hep G2 cells (detailed data are given in Table S15†), suggesting that they avoid the inflammatory responses associated with late apoptosis or necrosis. In comparison, **[$L_2Ti^{IV}Dipic$]** is prone to inducing late Hep G2 apoptosis (early/late apoptosis: 9.6%/22.7% at $1 \times 10^{2}$ μM). This has already been observed for **[$L_5Hf^{IV}Dipic^{4\text{-Cl}}$]**[30] and **[$L_2Ti^{IV}Dipic$]**[13] on HeLa S3 cells, which at $1 \times 10^{2}$ μM induced 30.5%(Hf)/20.8%(Ti) and 15.5%(Hf)/62.3%(Ti) of early and

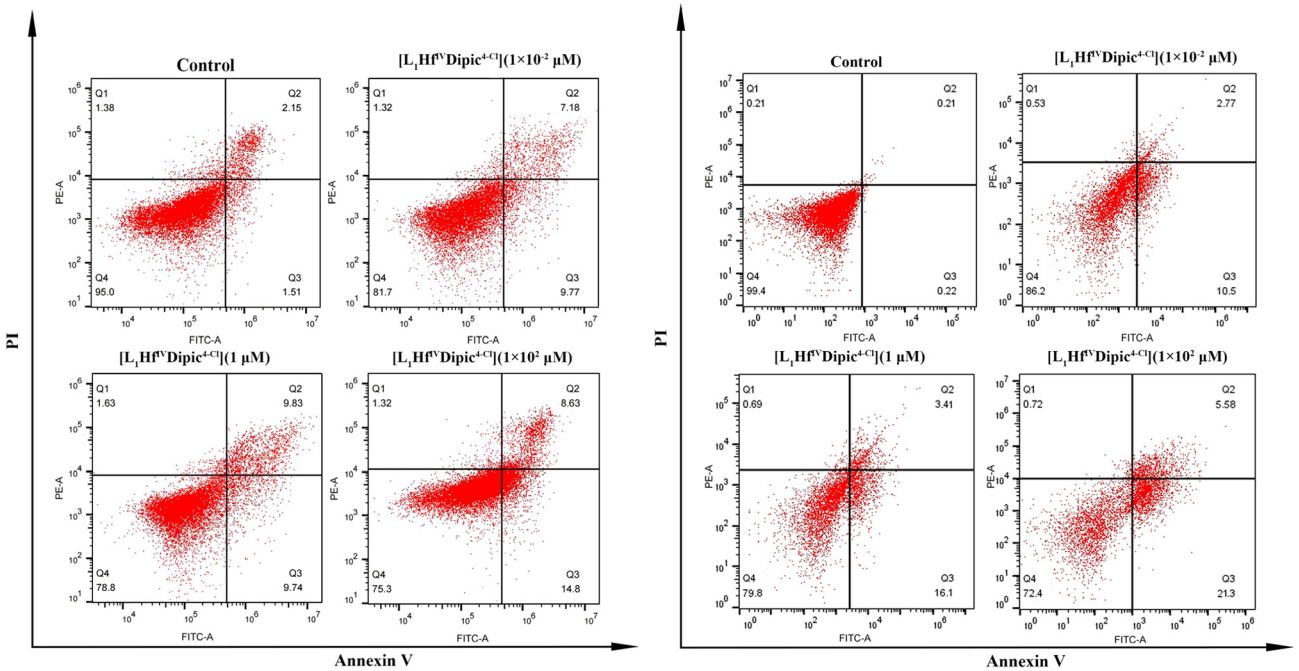


Fig. 3 Quantification of necrotic (Q1), late apoptotic (Q2), early apoptotic (Q3) and viable (Q4) HeLa S3 cells (left) and Hep G2 cells (right) after 24 h of incubation with control medium, $1 \times 10^{-2}$ μM, 1 μM and $1 \times 10^{2}$ μM **[$L_1Hf^{IV}Dipic^{4-Cl}$]**.

late apoptosis, respectively. Overall, the ability to induce early apoptosis seems to be a hallmark of Hf complexes.

### Inhibition of cell migration

Tumor migration or invasion is a major issue that needs to be addressed in cancer therapy, since it is responsible for metastasis, which is the primary cause of cancer-related mortality. In order to preliminarily examine the metastasis inhibition ability of the new $Hf^{IV}$ complexes, a wound healing assay of **[$L_1Hf^{IV}Dipic^{4-Cl}$]** and the previously reported **[$L_5Hf^{IV}Dipic^{4-Cl}$]** on HeLa S3 cells was performed. In brief, cells were incubated with each complex for 24 h, and the WCR (wound closure rate) was used for describing the metastasis inhibition activity (see eqn (S1)†). As depicted in Fig. 4a, the WCR of **[$L_1Hf^{IV}Dipic^{4-Cl}$]** and **[$L_5Hf^{IV}Dipic^{4-Cl}$]** were both concentration dependent, since at concentrations of 2 μM and 4 μM, the WCR values were 8.3% and 5.4% for **[$L_1Hf^{IV}Dipic^{4-Cl}$]**, and 9.5% and 7.6% for **[$L_5Hf^{IV}Dipic^{4-Cl}$]**, respectively (Fig. 4b; the detailed experimental procedure can be found in the ESI†), while for the control it was 14.6% at 24 h. Therefore, the results show that both complexes reduce the cellular migration of HeLa S3 cells.

### Cellular uptake

Next, we performed a cellular uptake investigation of **[$L_1Hf^{IV}Dipic^{4-Cl}$]** using HeLa S3 cells, following the procedure used in our previous report.[30] A total of $3 \times 10^{-9}$ mol of **[$L_1Hf^{IV}Dipic^{4-Cl}$]** ($2.26 \times 10^{-3}$ mg) was added to HeLa S3 cells, and samples taken at 10 min, 30 min, 1 h, 2 h, 24 h and 48 h were subjected to ICP-MS (inductively coupled plasma mass spectrometry) analysis for cellular Hf content. The percentages

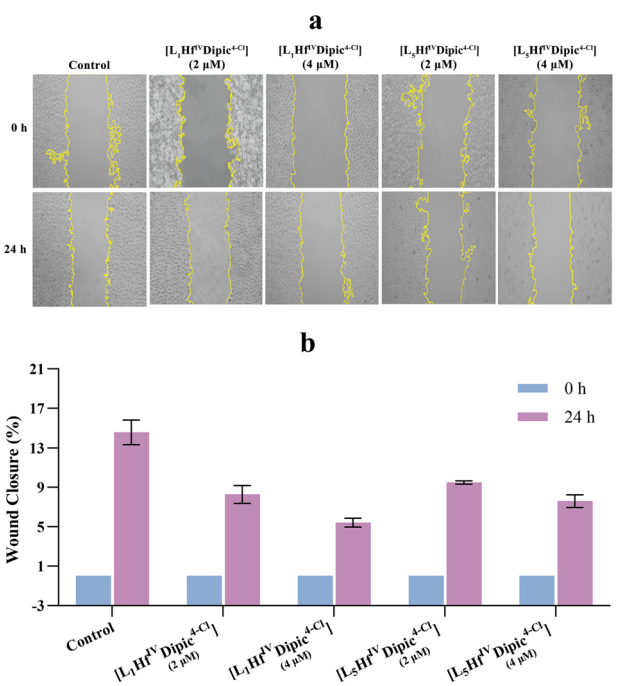


Fig. 4 (a) Representative images of the wound healing assay after 0 and 24 h of treatment of HeLa S3 cells with either **[$L_1Hf^{IV}Dipic^{4-Cl}$]** or **[$L_5Hf^{IV}Dipic^{4-Cl}$]**. (b) Quantitative data of wound closure percentages.

of cellular Hf in relation to total Hf were 3.55%, 4.86%, 5.97%, 7.09%, 8.22% and 8.59%, at each time point. Taking the cellular Hf amount at 48 h (46 ng) as the maximum uptake, 41.30% of the maximum Hf uptake was achieved after 10 min and

69.60% after 30 min (Fig. 5a). In comparison with [$L_5Hf^{IV}Dipic^{4\text{-}Cl}$], which showed 61.90% (10 min) and 76.20% (1 h) of the maximum Hf uptake (42 ng, 48 h),[30] it can be concluded that the initial Hf uptake of [$L_1Hf^{IV}Dipic^{4\text{-}Cl}$] is slower, but is similar or higher after one hour (Fig. 5b).

### Intracellular ROS assessments

Oxidative stress and accumulation of ROS (reactive oxygen species) including $^{\bullet}O_2^-$ (superoxide anion), HO$^{\bullet}$ (hydroxyl radical), $^1O_2$ (singlet oxygen) and $H_2O_2$ (hydrogen peroxide) are closely related to tumor formation and mitosis.[34] ROS at higher levels can lead to cell death, including apoptosis, autophagy, necroptosis or ferroptosis, with multiple cellular targets being involved.[35] In this study, the ROS production induced by [$L_1Hf^{IV}Dipic^{4\text{-}Cl}$] and [$L_5Hf^{IV}Dipic^{4\text{-}Cl}$] in HeLa S3 cells was examined with the 2′,7′-dichlorodihydro-fluorescein diacetate ($H_2$DCFDA probe)[36] (three repeats). $H_2$DCFDA is not fluorescent, but after reaction with ROS, it can be transformed into DCF (2′,7′-dichlorofluorescein), which shows green emission and can be detected by fluorescence microscopy. One representative experiment is depicted in Fig. 6. We found that both [$L_1Hf^{IV}Dipic^{4\text{-}Cl}$] and [$L_5Hf^{IV}Dipic^{4\text{-}Cl}$] could induce ROS generation at the two tested concentrations (1 μM and 2 μM). Moreover, the fluorescence in the case of [$L_1Hf^{IV}Dipic^{4\text{-}Cl}$] was much stronger in comparison with [$L_5Hf^{IV}Dipic^{4\text{-}Cl}$], indicating a higher level of ROS production with the former.

In order to find what types of ROS are generated in tumor cells, and the cellular effects for which they are responsible, an *in vitro* ROS investigation was conducted on HeLa S3 cells by flow cytometry. HeLa S3 cells were incubated with [$L_1Hf^{IV}Dipic^{4\text{-}Cl}$] followed by different ROS scavengers, namely $NaN_3$ ($^1O_2$ scavenger), Tiron (disodium 4,5-dihydroxybenzene-1,3-disulfonate, $^{\bullet}O_2^-$ scavenger), D-mannitol (HO$^{\bullet}$ scavenger) and Nap (sodium pyruvate, $H_2O_2$ scavenger). As depicted in Fig. 7, the fluorescence intensity of DCF was slightly reduced (<40%) in the $NaN_3$, Tiron and Nap groups when compared to the control (only with [$L_1Hf^{IV}Dipic^{4\text{-}Cl}$]), indicating that $^1O_2$, $^{\bullet}O_2^-$ and $H_2O_2$ are not the main ROS species formed. Obvious quenching of the DCF fluorescence (<80%) was observed in the D-mannitol group, suggesting that HO$^{\bullet}$ accounted for the majority of [$L_1Hf^{IV}Dipic^{4\text{-}Cl}$]-induced ROS.

Metal ions such as Cu, Fe, Mn and Ru can induce ROS generation through the Fenton reaction, the Haber–Weiss reaction, and mitochondrial dysfunction.[37] However, reports on how molecular Hf complexes induce ROS generation are scarce since Hf cannot easily undergo redox cycling, and is Fenton inactive. Hf loses all the outermost s and d electrons, leaving ionic sites with almost empty orbitals that are not able to catalyze oxygen-related reactions.[38] Hf-based materials such as nanoparticles of $HfO_2$ and Hf-based MOFs are RT (radio therapy) sensitive, and $Hf^{IV}$ can absorb X-ray energy and convert it to high-energy electrons, which subsequently interact with $H_2O$ to generate HO$^{\bullet}$.[39,40] It has been shown that mitochondrial ETC (electron transport chain) activity can lead to the production of ROS, including superoxide and hydroxyl radicals. In the process, the mitochondrial ETC transfers electrons to $O_2$, and $O_2$ is reduced to $^{\bullet}O_2^-$ anions, which are ultimately converted to hydroxyl radicals (HO$^{\bullet}$).[41] This mechanism may

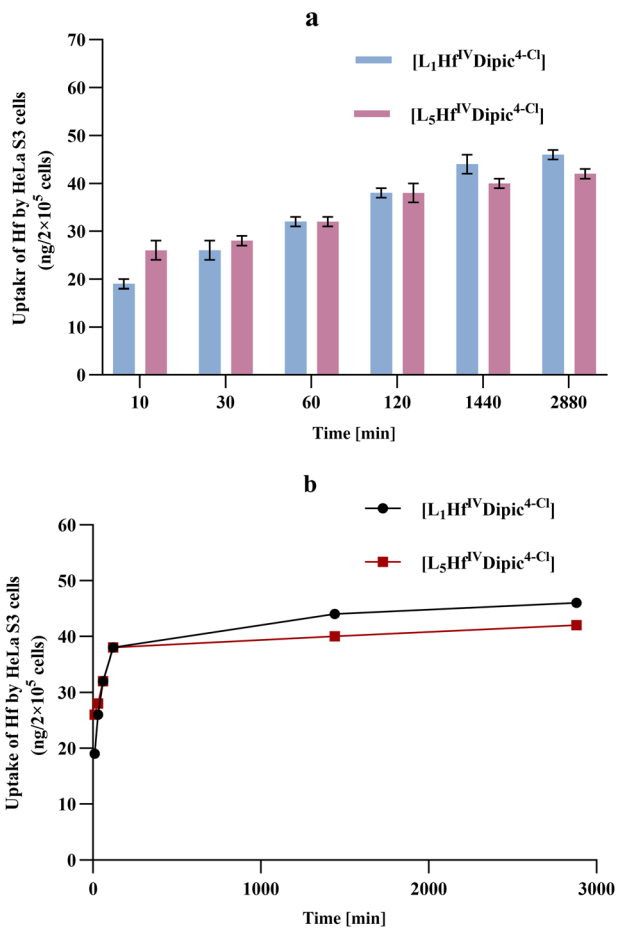


Fig. 5 (a) Cellular uptake of Hf after treating HeLa S3 cells for 10 min, 30 min, 1 h, 2 h, 24 h and 48 h with [$L_1Hf^{IV}Dipic^{4\text{-}Cl}$] (2 μM) and [$L_5Hf^{IV}Dipic^{4\text{-}Cl}$] (2 μM). Control group: HeLa S3 cells without treatment with [$L_1Hf^{IV}Dipic^{4\text{-}Cl}$] or [$L_5Hf^{IV}Dipic^{4\text{-}Cl}$], no Hf (0 ng) was detected by ICP-MS. (b) Fitted cellular uptake rate of Hf after treating HeLa S3 cells with [$L_1Hf^{IV}Dipic^{4\text{-}Cl}$] (2 μM) and [$L_5Hf^{IV}Dipic^{4\text{-}Cl}$] (2 μM).

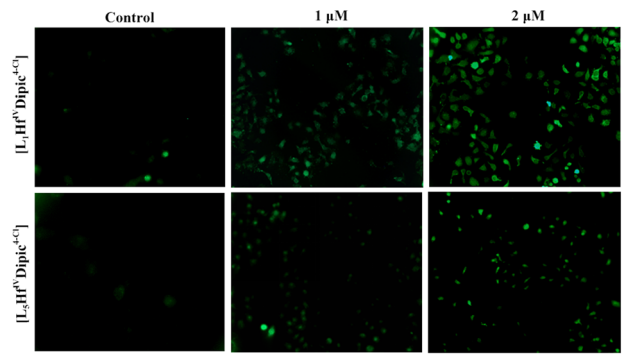


Fig. 6 Fluorescence microscopic images of intracellular ROS levels in HeLa S3 cells analyzed by the $H_2$DCFDA probe. The green spots are cells that are stained with DCF.

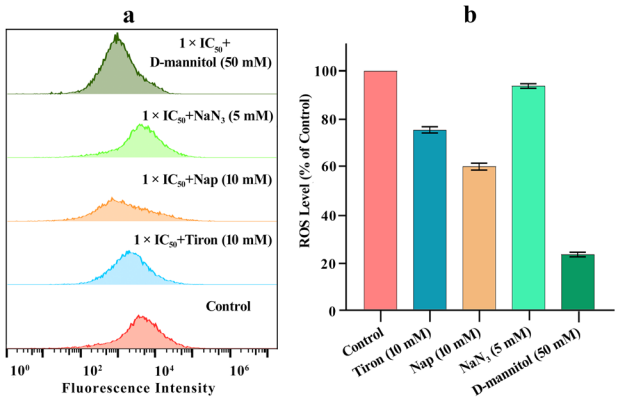


**Fig. 7** (a) Flow cytometry investigation of intracellular ROS levels analyzed with the $H_2$DCFDA probe in HeLa S3 cells treated with 2.2 μM [$L_1Hf^{IV}Dipic^{4\text{-}Cl}$] + different ROS scavengers for 24 h. (b) Fluorescence intensity of DCF in HeLa S3 cells treated with $NaN_3$, Tiron, D-mannitol and Nap.

explain how ROS are generated by [$L_1Hf^{IV}Dipic^{4\text{-}Cl}$]. Obviously, mitochondrial-related investigations are required to prove such a hypothesis.

### Mitochondrial membrane potential

Most of the production and conversion of $O_2$ and ATP takes place in the mitochondria, through oxidative phosphorylation, and the generated ROS can cause MMP (mitochondrial membrane potential) decrease and even mitochondrial dysfunction. Hence, MMP has been identified as an indicator of mitochondrial dysfunction and early cell apoptosis.[42] In this study, the MMP change of HeLa S3 cells treated with the two $Hf^{IV}$ complexes was investigated with the mitochondrial fluorescent cyanine tracer, JC-1 (5,5′,6,6′-tetrachloro-1,1′,3,3′-tetraethylbenzimi-dazolylcarbocyanine iodide).[43] JC-1 demonstrates red fluorescence when the mitochondrion is healthy and the MMP is unchanged. However, JC-1 can dissociate from the mito-

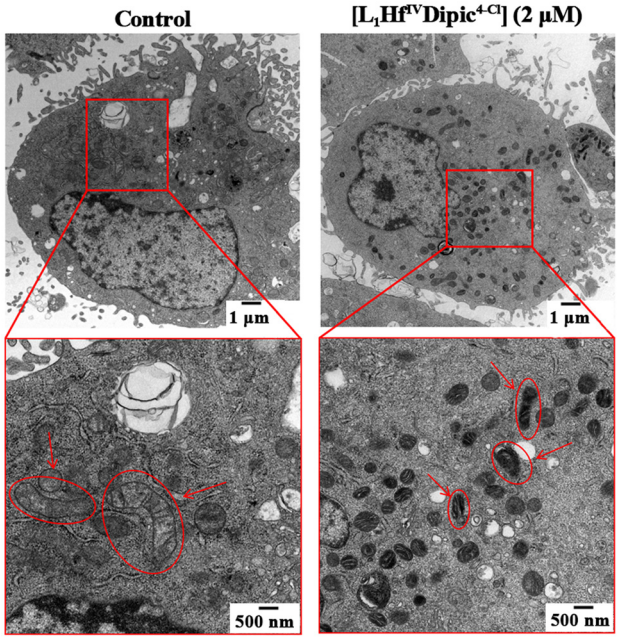


**Fig. 9** TEM images of HeLa S3 cells incubated with [$L_1Hf^{IV}Dipic^{4\text{-}Cl}$] (2 μM, 48 h). The images in the lower panels are enlarged from the red boxes in the upper panels. The mitochondria are highlighted by the red circles.

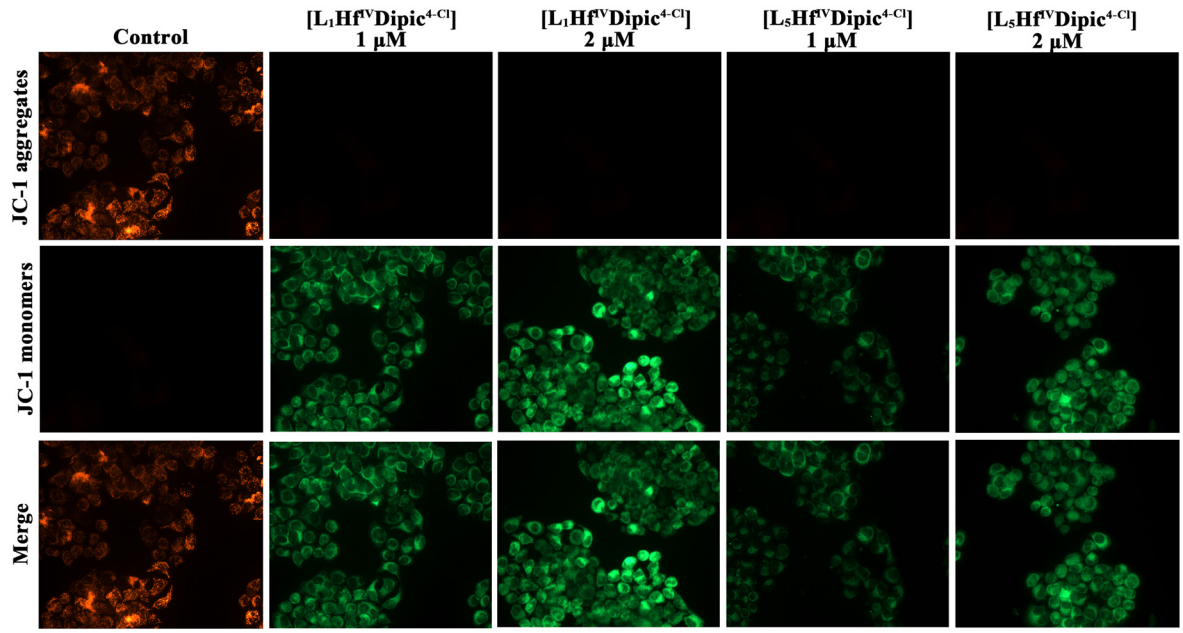


**Fig. 8** Staining of mitochondrial membrane potential in HeLa S3 cells after 24 h of treatment with different concentrations (1 μM and 2 μM) of complexes [$L_1Hf^{IV}Dipic^{4\text{-}Cl}$] and [$L_5Hf^{IV}Dipic^{4\text{-}Cl}$].

chondrial membrane with the fluorescence changing from red to green when the MMP decreases. In this study, HeLa S3 cells were incubated with the $Hf^{IV}$ complexes (at 1 μM and 2 μM) for 24 h and subsequently treated with the JC-1 staining solution. As depicted in Fig. 8, the MMP decreased in a concentration-dependent manner after treating HeLa S3 cells with [$L_1Hf^{IV}Dipic^{4\text{-}Cl}$] and [$L_5Hf^{IV}Dipic^{4\text{-}Cl}$]. Stronger green fluorescence could be observed for cells treated with [$L_1Hf^{IV}Dipic^{4\text{-}Cl}$] compared to [$L_5Hf^{IV}Dipic^{4\text{-}Cl}$], indicating that [$L_1Hf^{IV}Dipic^{4\text{-}Cl}$] could induce more ROS generation in HeLa S3 cells and most probably is more prone to inducing mitochondria dysfunction. This is in agreement with the study made with the $H_2$DCFDA probe.

Moreover, excessive ROS accumulation in mitochondria leads to structural changes that compromise their function.[41] As shown in Fig. 9, a transmission electron microscopy (TEM) analysis revealed that HeLa S3 cells treated with [$L_1Hf^{IV}Dipic^{4\text{-}Cl}$] exhibited pronounced mitochondrial damage, including atrophy and disrupted cristae. Typical apoptotic-related hyper-chromatin could be observed. In the control group, mitochondria maintained their normal tubular architecture—an intact outer membrane, clearly defined cristae, and no sign of edema or atrophy.

## Conclusions

In conclusion, eight novel [ONON]-type $Hf^{IV}$ bis-chelates containing tripodal-tetradentate $L_{1-4}$ and a common 2-picolylamino co-ligand were synthesized in good yields and high purity. The complexes were purified by flash chromatography or by extraction with organic solvents. Single-crystal X-ray diffraction studies indicate that these [ONON]-type $Hf^{IV}$ complexes have more flexible coordination spheres than the [ONNO] (Salan)-type $Hf^{IV}$ complexes. Similarly to the Salan-type $Hf^{IV}$ complexes, the [ONON]-type complexes remained stable in aqueous media when *t*-butyl groups are located at the *ortho*-position of the phenolato moiety. Most [ONON]-type $Hf^{IV}$ complexes showed a selective inhibitory effect against Hep G2 cells. Among them, the four complexes ([$L_{1-4}Hf^{IV}Dipic^{4\text{-}Cl}$]) containing the chloro-substituted Dipic co-ligand exhibit the strongest cytotoxicity. The SAR suggests that both ligands of the heteroleptic complex are crucial for bioactivity; *i.e.* the substitution on the Dipic can be used to adjust the molecular polarity, leading to enhanced solubility in polar solvents and higher cytotoxicity, and methyl groups on the phenolate also increase the activity. In comparison with the Salan-type $Hf^{IV}$ complexes, the cellular uptake of [ONON]-type $Hf^{IV}$ complexes is initially slower, but the total Hf uptake is higher. In addition, the ROS production of [$L_1Hf^{IV}Dpic^{4\text{-}Cl}$] is dose dependent and it outperformed [$L_5Hf^{IV}Dpic^{4\text{-}Cl}$] (Salan type). [$L_1Hf^{IV}Dpic^{4\text{-}Cl}$] selectively produces hydroxyl radicals ($HO^{\bullet}$) as the major ROS. Furthermore, [$L_{1,5}Hf^{IV}Dpic^{4\text{-}Cl}$] can cause mitochondrial dysfunction and MMP decrease, which may account for the ROS generation. Cell apoptosis (HeLa S3 and Hep G2) studies have provided some insight into the unexplored features of anti-tumor $Hf^{IV}$ complexes. An interesting finding is that both families of $Hf^{IV}$ complexes ([ONON] and [ONNO]) induce mostly early apoptosis, which is preferred because it causes less inflammation. Further investigations such as molecular modification, targeted therapy and detailed molecular mechanisms are currently underway in our laboratory.

## Author contributions

Tiankun Zhao: supervision, conceptualization. Qi Zhang: methodology, writing – original draft. Jialiu Zhao: investigation, validation. Dongyu Mei: investigation, validation. Jing Ma: data curation. Isabel Correia: data curation, writing – review & editing. Zhongduo Yang: writing – review & editing. Sa-Hyun Kim: resources, formal analysis. Thomas Huhn: supervision, conceptualization.

## Data availability

CCDC 2390816 ([$L_2Hf^{IV}Dipic$]) and 2390817 ([$L_2Hf^{IV}Dipic^{4\text{-}Cl}$]).† Supplementary data associated with this article can be found in the online version.†

## Conflicts of interest

The authors declare no conflict of interest.

## Acknowledgements

We are grateful to the Gansu College Teacher Innovation Project (2025A-035); the Gansu Technological Innovation Guidance Plan (24CXJA005); the National Natural Science Foundation of China (No. 22267011); and the project of the Bureau of Science and Technology of Lanzhou (2023-RC-43) for the funding of this project. The support provided by China Scholarship Council (CSC) during a visit of T. Zhao to University of Lisbon is acknowledged. I. C. thanks Fundação para a Ciência e a Tecnologia (FCT) through projects UIDB/00100/2020 (**https://doi.org/10.54499/UIDB/00100/2020**), UIDP/00100/2020 (**https://doi.org/10.54499/UIDP/00100/2020**), and LA/P/0056/2020 (**https://doi.org/10.54499/LA/P/0056/2020**). The authors thank Dr Xianggao Meng from Central China Normal University for useful discussion on the X-ray analysis.

## References

1 H. Köpf and P. Köpf-Maier, Titanocene Dichloride—The First Metallocene with Cancerostatic Activity, *Angew. Chem., Int. Ed. Engl.*, 1979, **18**(6), 477–478.
2 H. J. Keller, B. Keppler and D. Schmähl, Antitumor Activity of cis-Dihalogenobis(1-phenyl-1,3-butanedionato) Titanium

(IV) Compounds. A New Class of Antineoplastic Agents, *J. Cancer Res. Clin. Oncol.*, 1983, **105**(1), 109–110.
3 F. Caruso and M. Rossi, Antitumor Titanium Compounds, *Mini-Rev. Med. Chem.*, 2004, **4**(1), 49–60.
4 M. Shavit, D. Peri, C. M. Manna, J. S. Alexander and E. Y. Tshuva, Active Cytotoxic Reagents Based on Non-metallocene Non-diketonato Well-Defined $C_2$-Symmetrical Titanium Complexes of Tetradentate Bis(phenolato) Ligands, *J. Am. Chem. Soc.*, 2007, **129**(40), 12098–12099.
5 T. A. Immel, U. Groth and T. Huhn, Cytotoxic Titanium Salan Complexes: Surprising Interaction of Salan and Alkoxy Ligands, *Chem. – Eur. J.*, 2010, **16**(9), 2775–2789.
6 H. Glasner and E. Y. Tshuva, $C_1$-Symmetrical Titanium(IV) Complexes of Salan Ligands with Differently Substituted Aromatic Rings: Enhanced Cytotoxic Activity, *Inorg. Chem.*, 2014, **53**(6), 3170–3176.
7 M. Grützke, T. Zhao, T. A. Immel and T. Huhn, Heptacoordinate Heteroleptic Salan (ONNO) and Thiosalan (OSSO) Titanium(IV) Complexes: Investigation of Stability and Cytotoxicity, *Inorg. Chem.*, 2015, **54**(14), 6697–6706.
8 T. A. Immel, M. Grützke, A.-K. Späte, U. Groth, P. Öhlschläger and T. Huhn, Synthesis and X-ray structure analysis of a heptacoordinate titanium(IV)-bis-chelate with enhanced *in vivo* antitumor efficacy, *Chem. Commun.*, 2012, **48**(46), 5790–5792.
9 G. Nahari and E. Y. Tshuva, Synthesis of asymmetrical diaminobis(alkoxo)-bisphenol compounds and their $C_1$-symmetrical mono-ligated titanium(IV) complexes as highly stable highly active antitumor compounds, *Dalton Trans.*, 2021, **50**(19), 6423–6426.
10 R. Manne, M. Miller, A. Duthie, M. F. C. Guedes da Silva, E. Y. Tshuva and T. S. Basu Baul, Cytotoxic homoleptic Ti(IV) compounds of ONO-type ligands: synthesis, structures and anti-cancer activity, *Dalton Trans.*, 2019, **48**(1), 304–314.
11 T. Zhao, M. Grützke, K. H. Götz, T. Druzhenko and T. Huhn, Synthesis and X-ray structure analysis of cytotoxic heptacoordinate sulfonamide salan titanium(IV)-bis-chelates, *Dalton Trans.*, 2015, **44**(37), 16475–16485.
12 G. Nahari, O. Braitbard, L. Larush, J. Hochman and E. Y. Tshuva, Effective Oral Administration of Antitumorigenic Nanoformulated Titanium Complex, *ChemMedChem*, 2021, **16**(1), 108–112.
13 S. Li, X. Zhang, T. Zhao, N. Liu, Y. Zhang, P. Wang, Z. Yang and T. Huhn, Synthesis, in vitro antitumor evaluation and structure activity relationship of heptacoordinated aminobis(Phenolato) Ti(IV) complexes stabilized by 2,6-dipicolinic acid, *J. Biol. Inorg. Chem.*, 2024, **29**(3), 315–330.
14 Z. Shpilt, N. Melamed-Book and E. Y. Tshuva, An anticancer Ti(IV) complex increases mitochondrial reactive oxygen species levels in relation with hypoxia and endoplasmic-reticulum stress: A distinct non DNA-related mechanism, *J. Inorg. Biochem.*, 2023, **243**, 112197.
15 G. W. Severin, C. H. Nielsen, A. I. Jensen, J. Fonslet, A. Kjær and F. Zhuravlev, Bringing Radiotracing to Titanium-Based Antineoplastics: Solid Phase Radiosynthesis, PET and ex Vivo Evaluation of Antitumor Agent [$^{45}$Ti](salan)Ti(dipic), *J. Med. Chem.*, 2015, **58**(18), 7591–7595.
16 K. Pedersen, C. Baun, K. Nielsen, H. Thisgaard, A. Jensen and F. Zhuravlev, Design, Synthesis, Computational, and Preclinical Evaluation of $^{nat}$Ti/$^{45}$Ti-Labeled Urea-Based Glutamate PSMA Ligand, *Molecules*, 2020, **25**, 1104.
17 T. Zhao, P. Wang, M. Ji, S. Li, M. Yang and X. Pu, Post-Synthetic Modification Research of Salan Titanium bis-Chelates *via* Sonogashira Reaction, *Acta Chim. Sin.*, 2021, **79**(11), 1385–1393.
18 T. Zhao, P. Wang, N. Liu, S. Li, M. Yang and Z. Yang, Facile synthesis of [ONON] type titanium$^{(IV)}$ bis-chelated complexes in alcoholic solvents and evaluation of anti-tumor activity, *J. Inorg. Biochem.*, 2022, **235**, 111925.
19 T. Zhao, P. Wang, X. Zhang, N. Liu, W. Zhao, Y. Zhang, P. Yuan, S. Li, M. Yang, Z. Yang and T. Huhn, Anti-tumoral Titanium$^{(IV)}$ Complexes Stabilized with Phenolato Ligands and Structure-Activity Relationship, *Curr. Top. Med. Chem.*, 2023, **23**(19), 1835–1849.
20 B. Yu, Z.-H. Zhu, W.-W. Qin, H.-L. Wang, Y.-L. Li, F.-P. Liang and H.-H. Zou, Enhancement of Luminescence, Multiple-Sensing, and Differentiated Live-Cell-Imaging Properties of High-Nuclear Lanthanide Nanoclusters via the Zn(II)-Chelate-Controlled Dual Antenna Effect, *ACS Mater. Lett.*, 2024, **6**(8), 3312–3326.
21 S. Garon, E. K. C. Lau, S.-L. Chew, S. T. Lee and M. E. Thompson, Metal (IV) tetras (8-hydroxyquinoline)(M = Zr, Hf) used as electroluminescent material and electron-transport layer in OLEDs, *J. Soc. Inf. Disp.*, 2005, **13**(5), 405–409.
22 A. J. Chmura, M. G. Davidson, M. D. Jones, M. D. Lunn, M. F. Mahon, A. F. Johnson, P. Khunkamchoo, S. L. Roberts and S. S. F. Wong, Group 4 Complexes with Aminebisphenolate Ligands and Their Application for the Ring Opening Polymerization of Cyclic Esters, *Macromolecules*, 2006, **39**(21), 7250–7257.
23 S. L. Hancock, M. F. Mahon, G. Kociok-Kőhn and M. D. Jones, Homopiperazine and Piperazine Complexes of ZrIV and HfIV and Their Application to the Ring-Opening Polymerisation of Lactide, *Eur. J. Inorg. Chem.*, 2011, **2011**(29), 4596–4602.
24 M. Mandal, V. Ramkumar and D. Chakraborty, Salen complexes of zirconium and hafnium: synthesis, structural characterization and polymerization studies, *Polym. Chem.*, 2019, **10**(25), 3444–3460.
25 K. Press, V. Venditto, I. Goldberg and M. Kol, Zirconium and hafnium Salalen complexes in isospecific polymerisation of propylene, *Dalton Trans.*, 2013, **42**(25), 9096–9103.
26 P. Köpf-Maier, B. Hesse and H. Köpf, Tumor Inhibition by Metallocenes: Effect of Titanocene, Zirconocene, and Hafnocene Dichlorides on Ehrlich Ascites Tumor in Mice, *J. Cancer Res. Clin. Oncol.*, 1980, **96**(1), 43–51.
27 A. A. El-Habeeb, Novel Gallium(III), Germanium(IV), and Hafnium(IV) Folate Complexes and Their Spectroscopic, Thermal Decomposition, Morphological, and Biological Characteristics, *Bioinorg. Chem. Appl.*, 2020, **2020**, 6678688.

 

28 R. M. Lord, J. J. Mannion, A. J. Hebden, A. E. Nako, B. D. Crossley, M. W. McMullon, F. D. Janeway, R. M. Phillips and P. C. McGowan, Mechanistic and Cytotoxicity Studies of Group IV β-Diketonate Complexes, *ChemMedChem*, 2014, **9**(6), 1136–1139.

29 E. Choi, M. Landry, N. Pennock, M. Neufeld, K. Weinfurter, A. Goforth, J. Walker and C. Sun, Nanoscale Hafnium Metal–Organic Frameworks Enhance Radiotherapeutic Effects by Upregulation of Type I Interferon and TLR7 Expression, *Adv. Healthcare Mater.*, 2023, **12**, 2202830.

30 T. Zhao, P. Wang, N. Liu, W. Zhao, M. Yang, S. Li, Z. Yang, B. Sun and T. Huhn, Synthesis and X-ray structure analysis of cytotoxic heptacoordinated Salan hafnium$^{(IV)}$ complexes stabilized with 2,6-dipicolinic acid, *J. Inorg. Biochem.*, 2023, **240**, 112094.

31 W. Zhao, P. Yuan, Q. Zhang, N. Liu, Y. Wang, P. Wang, T. Huhn, Z. Yang and T. Zhao, Novel bimetallic oxido-bridged phenolato hafniumIV complex with enhanced anti-tumor activity and aqueous stability, *Results Chem.*, 2023, **6**, 101161.

32 J. Wang, J. Pan, Y. Tang, J. Chen, X. Fei, W. Xue and X. Liu, Advances of hafnium based nanomaterials for cancer theranostics, *Front. Chem.*, 2023, **11**, 1283924.

33 S. Ding, L. Chen, J. Liao, Q. Huo, Q. Wang, G. Tian and W. Yin, Harnessing Hafnium-Based Nanomaterials for Cancer Diagnosis and Therapy, *Small*, 2023, **19**(32), 2300341.

34 G. de la Riva Alberto, F. López Mendoza Javier and G. Agüero-Chapin, Known Hepatoprotectors Act as Antioxidants and Immune Stimulators in Stressed Mice: Perspectives in Animal Health Care, *Curr. Pharm. Des.*, 2018, **24**(40), 4825–4837.

35 M. Azmanova and A. Pitto-Barry, Oxidative Stress in Cancer Therapy: Friend or Enemy?, *ChemBioChem*, 2022, **23**(10), e202100641.

36 M. Oparka, J. Walczak, D. Malinska, L. M. P. E. Van Oppen, J. Szczepanowska, W. J. H. Koopman and M. R. Wieckowski, Quantifying ROS levels using CM-$H_2$DCFDA and HyPer, *Methods*, 2016, **109**, 3–11.

37 Z.-H. Zhu, L. Zhang, S. Jia, Z. Ni, Y.-L. Li, H.-H. Zou, Y. Yang, Y. Hu, D. Ding, B. Z. Tang and G. Feng, Nanoscale Metal-Organic Framework Leveraging Water, Oxygen, and Hydron Peroxide to Generate Reactive Oxygen Species for Cancer Therapy, *Adv. Funct. Mater.*, 2025, 2419548.

38 B. Ji, J. Gou, Y. Zheng, X. Pu, Y. Wang, P. Kidkhunthod and Y. Tang, Coordination Chemistry of Large-Sized Yttrium Single-Atom Catalysts for Oxygen Reduction Reaction, *Adv. Mater.*, 2023, **35**(24), 2300381.

39 Y. Chen, S. Liu, P. Gao, M. Shi, W. Pan, N. Li and B. Tang, NIR-II light-assisted radiotherapy based on ultrasmall $HfO_2$-embedded porous carbon nanooctahedra for overcoming tumor radioresistance, *Mater. Today Nano*, 2022, **20**, 100253.

40 Y. Zhao, C. Liang, Z. Mei, H. Yang, B. Wang, C. Xie, Y. Xu and J. Tian, Oxygen-Enriched MOF-Hemoglobin X-ray Nanosensitizer for Enhanced Cancer Radio–Radiodynamic Therapy, *ACS Mater. Lett.*, 2023, **5**(12), 3237–3247.

41 F. R. Palma, B. N. Gantner, M. J. Sakiyama, C. Kayzuka, S. Shukla, R. Lacchini, B. Cunniff and M. G. Bonini, ROS production by mitochondria: function or dysfunction?, *Oncogene*, 2024, **43**(5), 295–303.

42 K. Facecchia, L. A. Fochesato, S. D. Ray, S. J. Stohs and S. Pandey, Oxidative Toxicity in Neurodegenerative Diseases: Role of Mitochondrial Dysfunction and Therapeutic Strategies, *J. Toxicol.*, 2011, **2011**, 683728.

43 A. Perelman, C. Wachtel, M. Cohen, S. Haupt, H. Shapiro and A. Tzur, JC-1: alternative excitation wavelengths facilitate mitochondrial membrane potential cytometry, *Cell Death Dis.*, 2012, **3**(11), e430.